



1 Introduction

30 Snow cornices are overhanging projections of snow forming due to the deposition of wind transported snow in the lee of
ridgelines or sharp slope inflections (Montagne et al., 1968; Seligman, 1936). Cornices have attracted interest for their
hydrologic implications (e.g. Anderton et al., 2004) and as agents of geomorphic change in periglacial environments
(Eckerstorfer et al., 2013; Humlum et al., 2007), but are perhaps best recognized as a snow and avalanche hazard in
mountainous terrain (Montagne et al., 1968; Vogel et al., 2012). Cornices pose an avalanche hazard when they fail either as a
35 full cornice failure with the entire cornice detaching from the ground or as a partial failure with a smaller cornice mass
separating from the rest of the cornice. The detached cornice blocks travel downslope under the influence of gravity and
become a cornice fall avalanche by entraining loose surface snow or triggering a snow slab on the slope below (e.g. Vogel et
al., 2012). In ski areas or where cornices and cornice fall avalanches endanger infrastructure, both explosives (Farizy,
2013; McCarty et al., 1986) and structural defenses (e.g. Montagne et al., 1968) are employed operationally to mitigate
40 cornice hazard. Most cornice-related fatalities, however, occur in recreational backcountry settings and result from the
victim's weight triggering cornice failure.

Despite the well-recognized hazards and operational challenges associated with cornices and cornice fall avalanches, specific
cornice research is relatively scarce. Early cornice studies summarized by Vogel et al. (2012) focused on qualitative
descriptions of cornice formation processes and resulting cornice structures (e.g. Montagne et al., 1968; Seligman, 1936).
45 Later studies investigated mechanisms by which individual snow crystals adhere during cornice accretion (Latham and
Montagne, 1970), the physical snow characteristics at various structural locations on individual cornices (Naruse et al.,
1985), and the specific interactions between wind-drifted snow and cornice morphology during cornice formation
(Kobayashi et al., 1988).

Recent work has refined the conceptual model of seasonal cornice dynamics established by these earlier studies primarily by
50 employing time-lapse photography to examine cornice responses to the meteorological factors controlling the development
and failure of cornices (Munroe, 2018; van Herwijnen and Fierz, 2014; Vogel et al., 2012). Vogel et al. (2012) observed
cornice processes over two winter seasons on a single mountain slope in central Svalbard and proposed a conceptual model
of seasonal cornice dynamics including cornice accretion, deformation, and failure. Their results indicated cornice accretion
occurs during or immediately following winter storms with wind speeds in excess of 10 m s^{-1} from a direction perpendicular
55 to the ridgeline, while cornice scouring resulted from strong winds oriented towards the cornice's leading edge. Smaller
cornice failures observed in this study were clustered in June near the end of the snow season and coincided with increasing
air temperatures and decreased snow strength. Less frequent failures in the earlier part of the winter often involved the entire
cornice mass and resulted in the some of the largest cornice fall avalanches observed in the study.

Later work in an alpine setting also linked cornice accretion to strong winds during or soon after a snowfall and found the
60 **SNOWPACK** wind drift index correlated well with cornice width estimates (van Herwijnen and Fierz, 2014). No cornice

Kommentarzusammenfassung: Hancock_Review_nhess-2019-329.pdf

Seite:2

 Autor: FEY_C Betreff: Hervorheben Datum: 19-11-2019 15:12:29

 Autor: FEY_C Betreff: Hinweis Datum: 19-11-2019 15:13:22
You mean the study of Vogel et al.?

 Autor: FEY_C Betreff: Hervorheben Datum: 19-11-2019 15:11:42

 Autor: FEY_C Betreff: Hinweis Datum: 19-11-2019 15:12:27
???



failures or cornice fall avalanches were observed in this study, however. Munroe (2018) used time-lapse photography to observe the growth and repeated failure of a cornice in Utah, USA. He also found cornice accretion to primarily coincide with periods of snowdrift. He divided the nineteen cornice fall avalanches observed in his study into two distinct groups: snow-caused cornice fall avalanches where failure primarily resulted from snow loading on the cornice and temperature-
65 caused avalanches where failure is related to rapid temperature increases presumably leading to destabilization of the cornice through the loss of snow strength.

We build upon the observational understanding and conceptual model of seasonal cornice dynamics established in these previous works by monitoring cornice systems in Longyeardalen – including one site previously examined by Vogel et al. (2012) – with a terrestrial laser scanner (TLS). TLS – or ground-based LiDAR (Light detection and ranging) – is an active
70 remote sensing technology with documented applications for observing and monitoring various slope processes and hazards including landslides (Jaboyedoff et al., 2012; Prokop and Panholzer, 2009), coastal cliff erosion (e.g. Caputo et al., 2018), and rock slope instability (Abellán et al., 2014). TLS is being increasingly employed in snow and avalanche research to map snow depth and snow depth change (e.g. Deems et al., 2013; Fey et al., 2019; Prokop, 2008; Schirmer et al., 2011). Other specific snow-related applications include quantifying snow drift processes to verify physical models (Mott et al.,
75 2011; Schön et al., 2015; Vionnet et al., 2014), observing avalanche activity to calibrate dynamic avalanche models (Prokop et al., 2015), assisting avalanche control operations (Deems et al., 2013), and as a tool in planning snow drift control fences (Prokop and Procter, 2016).

We monitored cornice accretion, deformation, failure, and associated cornice fall avalanche activity near Longyearbyen, Svalbard with TLS technology over two winter seasons (2016/2017 and 2017/2018). To our knowledge TLS has not been
80 employed to specifically monitor cornice dynamics, so our primary objectives are to use the high spatial resolution snow surface data acquired via TLS to:

1. Demonstrate the utility of TLS to observe cornice processes
2. Observe and quantify cornice accretion, deformation, failure, and associated cornice fall avalanches and link these processes to their controlling meteorological factors.
- 85 3. Use our findings to provide suggestions for forecasting cornice fall avalanches in this and other locations threatened by cornices.

2 Study Area

Figure 1 here

The present study focuses on the cornices forming above the Longyear valley (hereafter: Longyeardalen) in central Svalbard
90 (Figure 1). Longyeardalen is a glacially sculpted, u-shaped valley with a northeast/southwest oriented valley axis running



???

approximately 3 km from the termini of two small mountain glaciers to a fjord. The Gruvefjellet and Platåberget plateaus border Longyeardalen to the west and east, respectively, with Svalbard's administrative center, Longyearbyen, situated in the valley bottom. The Gruvefjellet and Platåberget slopes lie within the horizontally-bedded, lower-Tertiary aged Van Mijenfjord Group of sandstones and shales (Major, 2001). Resistant strata within this group form the area's extensive plateau topography. The entire region is underlain by continuous permafrost (Humlum et al., 2003).

Figure 2 here

We investigated seasonal cornice dynamics and cornice fall avalanches along and under the Gruvefjellet and Platåberget plateau margins, respectively (Figure 2). The steep valley walls descending from the broad plateau summits (approximately 450 m elevation) are characterized in their upper portions by protruding resistant bedrock buttresses and transport couloirs incised by fluvial and gravitational slope processes. The Gruvefjellet slope described in detail by Eckerstorfer et al. (2013) consists of a 50-70 m near-vertical bedrock cliff situated **between under** the plateau margin and over a 40-50° slope that serves as a slab avalanche release area. This broad slope transitions into the transport couloirs which in turn feed extensive avalanche fan deposits downslope. Similar morphology exists on the Platåberget slope, but the plateau margin transitions directly into discrete 45-55° release areas leading into the couloirs and lacks the near-vertical bedrock face present on Gruvefjellet.

Central Svalbard's climate is cold and arid, with a mean annual air temperature of -4.6°C and mean annual precipitation of 191 mm at the Svalbard Airport automated weather station (AWS) for the 1981-2010 period of record (Førland et al., 2011). Combined mean winter (DJF) and mean spring (MAM) precipitation for 1981-2010 is 86 mm (Førland et al., 2011). Mean winter air temperature for the same period is -11.7°C and mean spring air temperature is -8.3°C (Førland et al., 2011). Rapidly increasing air temperatures in the winter and spring in response to decreased sea ice extent (Isaksen et al., 2016) create difficulties establishing representative baseline temperature conditions, with recent reports indicating warming on the order of 3-5°C for Svalbard as a whole from 1971 to 2017 (Hanssen-Bauer et al., 2019). Less clear changes are apparent in the precipitation trends (e.g. Hanssen-Bauer et al., 2019), but mid-winter rain-on-snow events are dramatically increasing in frequency (e.g. Vikhamar-Schuler et al., 2016).

Svalbard's climatic situation prohibits the growth of woody vegetation, and snow distribution across the landscape is strongly controlled by the wind (e.g. Jaedicke and Sandvik, 2002). Southeasterly winds generally prevail across the region's plateau mountains, but often switch to westerly or southwesterly during winter storms and are frequently redirected along the major valley axes at lower elevations (Christiansen et al., 2013). Winter weather in central Svalbard fluctuates between extended periods of cold, stable high pressure punctuated by warm, wet low pressure systems conveyed northwards along the North Atlantic cyclone track (Hanssen-Bauer et al., 1990; Rogers et al., 2005). This is reflected in the region's snow and avalanche climate, where the snowpack typically consists of persistent weak layers formed during high pressure interspersed with wind slabs or ice layers formed during snow storms or rain-on-snow events (Eckerstorfer and Christiansen, 2011a).



We pre-processed the raw point clouds in RiSCAN Pro, Riegl's proprietary data processing software. We established a suite of ground control points on both Platåberget and Gruvefjellet using a differential global positioning system (DGPS) which we used to georeferenced individual point point clouds. We then aligned repeated snow-covered scans to the snow-free scans established in September 2016 using these ground control points and the "Multi Station Adjustment" plugin in RiSCAN Pro following the approach outlined by Prokop and Panholzer (2009). The 3D accuracy of this registration process ranged from <1 mm to 70 mm (Appendix 1). We then manually filtered non-ground points or points above the snow surface. Finally, we resampled the resulting point clouds to a 0.10 m grid and exported to an XYZ text file.

We imported individual point clouds into CloudCompare (CloudCompare, 2019), for further analyses (Figure 3). To create 2D cornice profile cross-sections, we extracted point cloud profile sections along manually defined axes using the polyline extraction tool native to CloudCompare (Figure 3c,d). This tool requires user-defined inputs for profile type, section thickness, and maximum edge length which we set to "Both", 0.6 m, and 0.2 m, respectively. We then manually edited and digitized the resulting shapefiles in the ArcScene 3D Editing environment (ArcGIS 10.4.1) to create the vertical cornice profile schematics as 3D shapefiles.

We calculated representative volumes for selected areas from both the Platåberget and Gruvefjellet cornice systems using the "Compute 2.5D Volume tool" in CloudCompare. This tool computes the volume between two 2.5D point clouds by rasterizing the point clouds to a specified grid size and then computing volumes based on the differences in a specified projection direction between the rasterized values (Figure 3 e,f,g,h). In our case, we rasterized our point clouds to a 1 m grid and calculated horizontal distance differences along the "X" projection direction, which in our georeferenced point clouds corresponds to east-west (i.e. the slope fall-lines). For each cornice system, we computed the volume of snow in 40 m x 8 m area of the plateau margin for each usable snow surface scan by subtracting the bare-earth surface from the scanned snow surface (Figure 3 e,f,g). We chose this areal extent to maximize coverage of an individual cornice throughout its development during the season (i.e. to completely capture the vertical extension of the leading edge) while minimizing volume changes related to other snow on the slope.

Figure 3 here

We used the Multiscale Model to Model Cloud Comparison (M3C2) algorithm developed by Lague et al. (2013) and implemented as a plugin in CloudCompare to quantify changes to the cornices and snow surfaces on the slopes below in 3D. The M3C2 algorithm allows for direct comparison of point clouds in 3D and is specifically developed to handle 3D differences and detect changes to complex surfaces where both vertical and horizontal changes exist (Lague et al., 2013). This functionality requires the user to input the following parameters: the normal scale, the projection scale, and the maximum depth (e.g. Lague et al., 2013; Watson et al., 2017). We selected a normal scale of 2 m oriented positively to the scan position (i.e. the normals "face" the scan position), a projection scale of 1 m, and a maximum depth of 10 m for all M3C2 calculations.

Seite:6

Autor: FEY_C Betreff: Hervorheben Datum: 19-11-2019 15:16:25

Autor: FEY_C Betreff: Hinweis Datum: 19-11-2019 15:19:07

The values gives from the RiScan MSA are not the 3D accuracy and does only reflect the distance between the point correspondences used at the ICP. I would neglect this value because it says nothing about the registration quality

Autor: FEY_C Betreff: Hervorheben Datum: 19-11-2019 15:19:18

Autor: FEY_C Betreff: Hinweis Datum: 19-11-2019 15:20:18

you mean the point cloud was thinned by blockthinning? the term "grid" is misleading with raster data.

Autor: FEY_C Betreff: Hervorheben Datum: 19-11-2019 15:22:57

add "

Autor: FEY_C Betreff: Hervorheben Datum: 19-11-2019 15:21:29



185 TLS-based snow surface measurement accuracy generally decreases with increasing distance from the scanner to the
measured snow surface and is affected by the manner in which the laser beam interacts with the snow surface, the local
terrain characteristics, the stability of the scanner while scanning, and the quality of the scan data registration process (Fey et
al., 2019;Hartzell et al., 2017;Prokop et al., 2008). The relative accuracy – the deviation between measurements of an
unchanged surface taken under different measurement conditions – can be assessed to quantify uncertainties related to both
190 registration errors and positional errors from the interaction of the laser beam with the surface (Fey et al., 2019;Prokop and
Panholzer, 2009). We assessed relative accuracy for our data by measuring M3C2 distances between each snow covered
scan and the snow-free scan on a 10x10 m area of stable, snow-free rock faces near the cornices on both Gruvefjellet and
Platåberget (Figure 2). We report relative accuracy for each snow-covered scan as the mean of all M3C2 distances on the
10x10 m area (Appendix 1) Locations for relative accuracy assessment were selected based on their ability to remain
functionally snow-free throughout the study and because they were not otherwise used in the registration process. As both
195 registration and positional errors can be spatially variable across the scanned area (Fey et al., 2019;Hartzell et al.,
2017;Prokop, 2008), we used these locations in close proximity to the cornices of interest to best represent the relative
accuracy near the cornices. Mean M3C2 distance values
are smaller than 80 mm for all scans, with standard deviations ranging from <10 mm to 72 mm (Appendix 1). Uncertainty
associated with the relative volume metric, calculated by multiplying the relative accuracy of each scan by the surface area
200 considered in the volume calculations (369 m²) thus ranged from less than 1 m³ to 28 m³ (Appendix 1).

3.3 Supplemental Observational Data

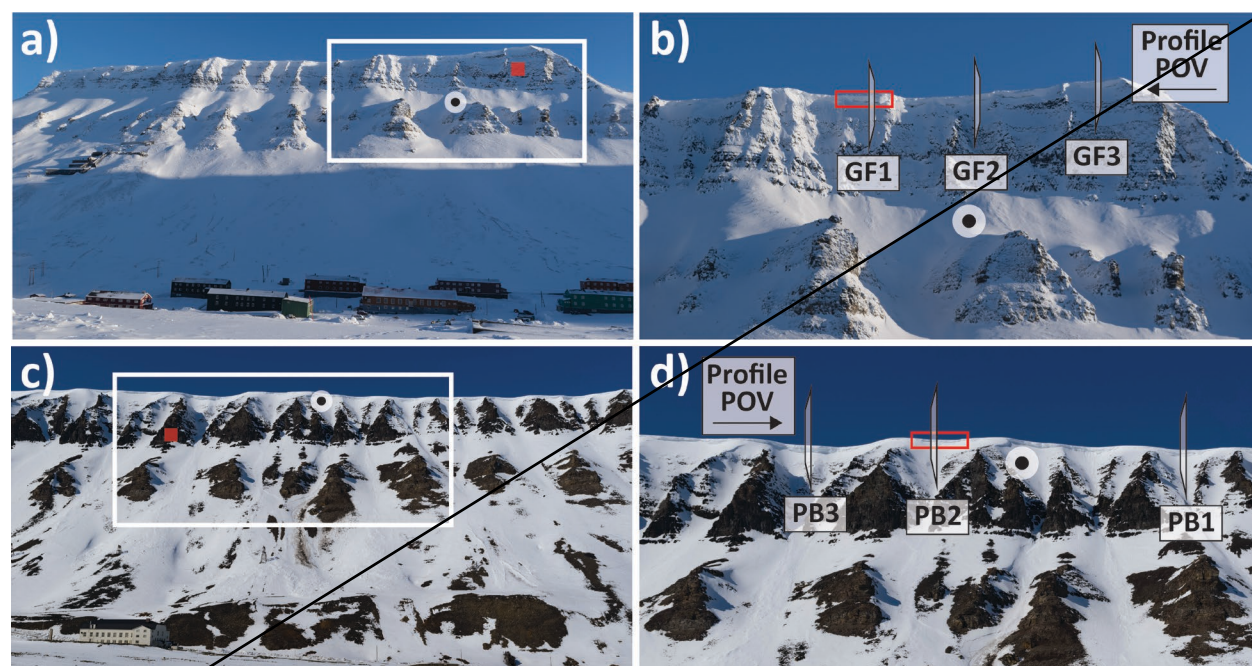
We relied on snow and avalanche observations from Platåberget and Gruvefjellet from the Norwegian Water Resources and
Energy Directorate's (NVE) online observation platform regObs (www.regobs.no) to supplement our TLS observations.
Local observers conduct snow and avalanche assessments on the Gruvefjellet and Platåberget slopes on a sub-weekly basis,
205 so we were able to much better constrain avalanche cycle timing than with the temporal resolution available from the TLS
data.

4 Results

4.1 Seasonal summaries

4.1.1 2016/2017

210 We compare seasonal meteorological conditions (Figure 4) with cross-sectional cornice profiles derived from eight scanned
snow surfaces on Gruvefjellet and seven surfaces on Platåberget. We selected these profiles from a pool of 18 usable scans
from Gruvefjellet and 14 from Platåberget (Appendix 1) to represent key points in the development of the cornice systems.



635 **Figure 2.** Overview of the cornice systems and locations of the primary spatial data employed in this work. Panel (a) shows Gruvefjellet
from SP1 taken on 21 March 2017, with the white rectangle approximating the 600 m horizontal extent of panel (b) and the red square
showing the area used to assess relative accuracy. Panel (b) indicates the location of the 2D cross-sectional profiles GF1, GF2, and GF3 in
addition to outlining the area used to calculate representative cornice volume in red. Panel (c) shows Platåberget from SP4 taken on 24
640 May 2017, with the white rectangle approximating the 600 m horizontal extent of panel (d) and the red square showing the area used to
assess relative accuracy. Panel (d) indicates the location of the 2D cross-sectional profiles PB1, PB2, and PB3 in addition to outlining the
area used to calculate representative cornice volume in red. Snow depth sensor locations are indicated in all panels with the black dot.

- Revise the color scheme of the profile to distinguish between the dates.

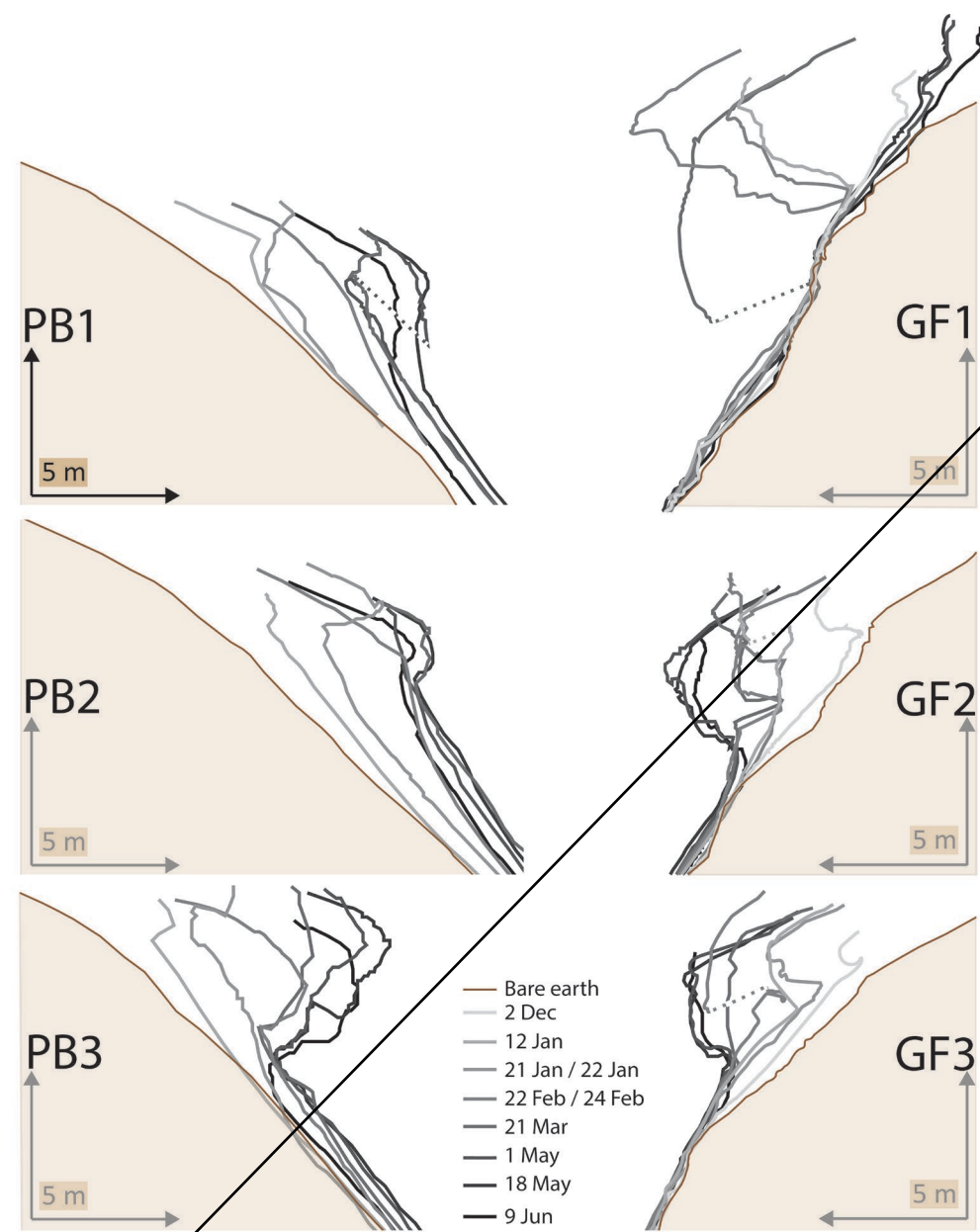
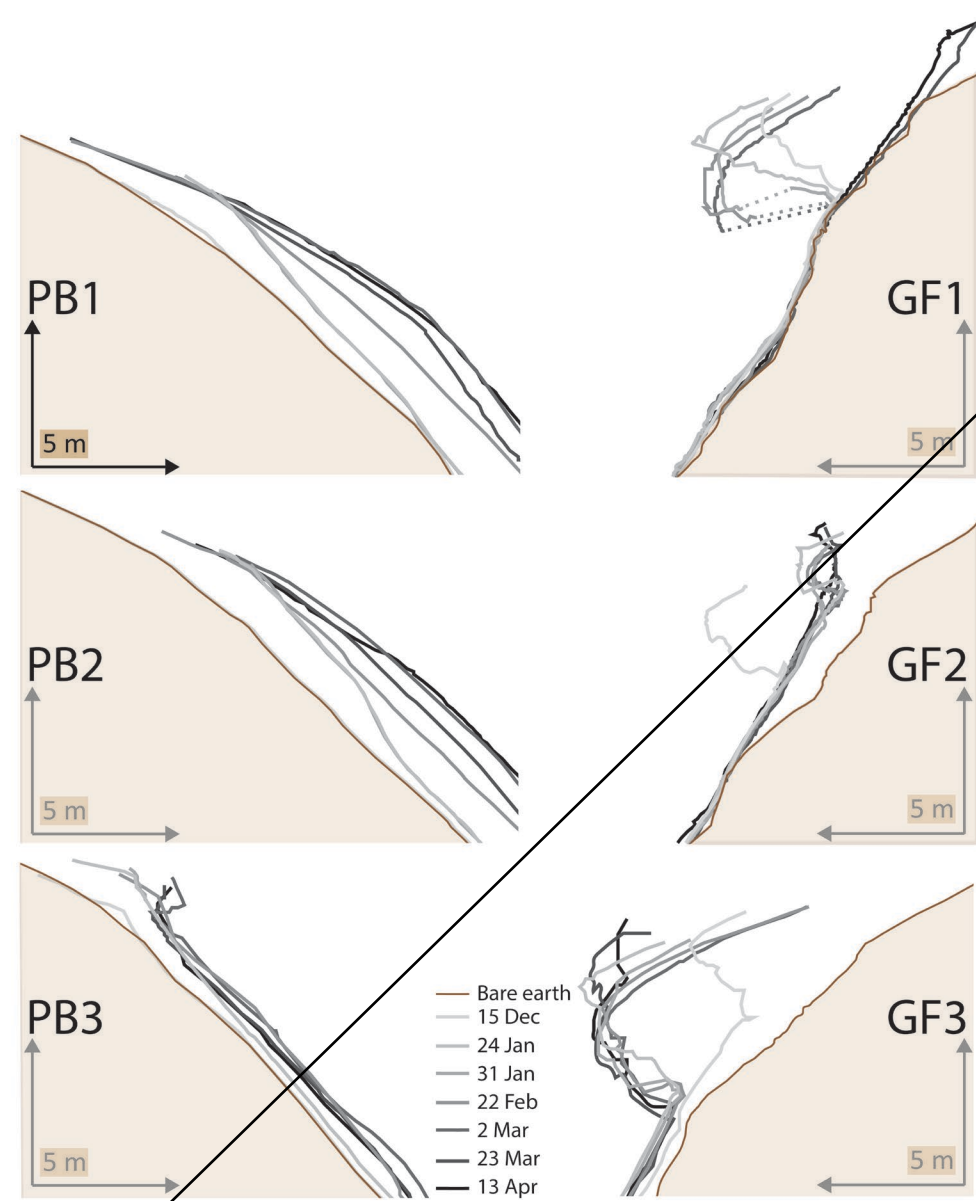


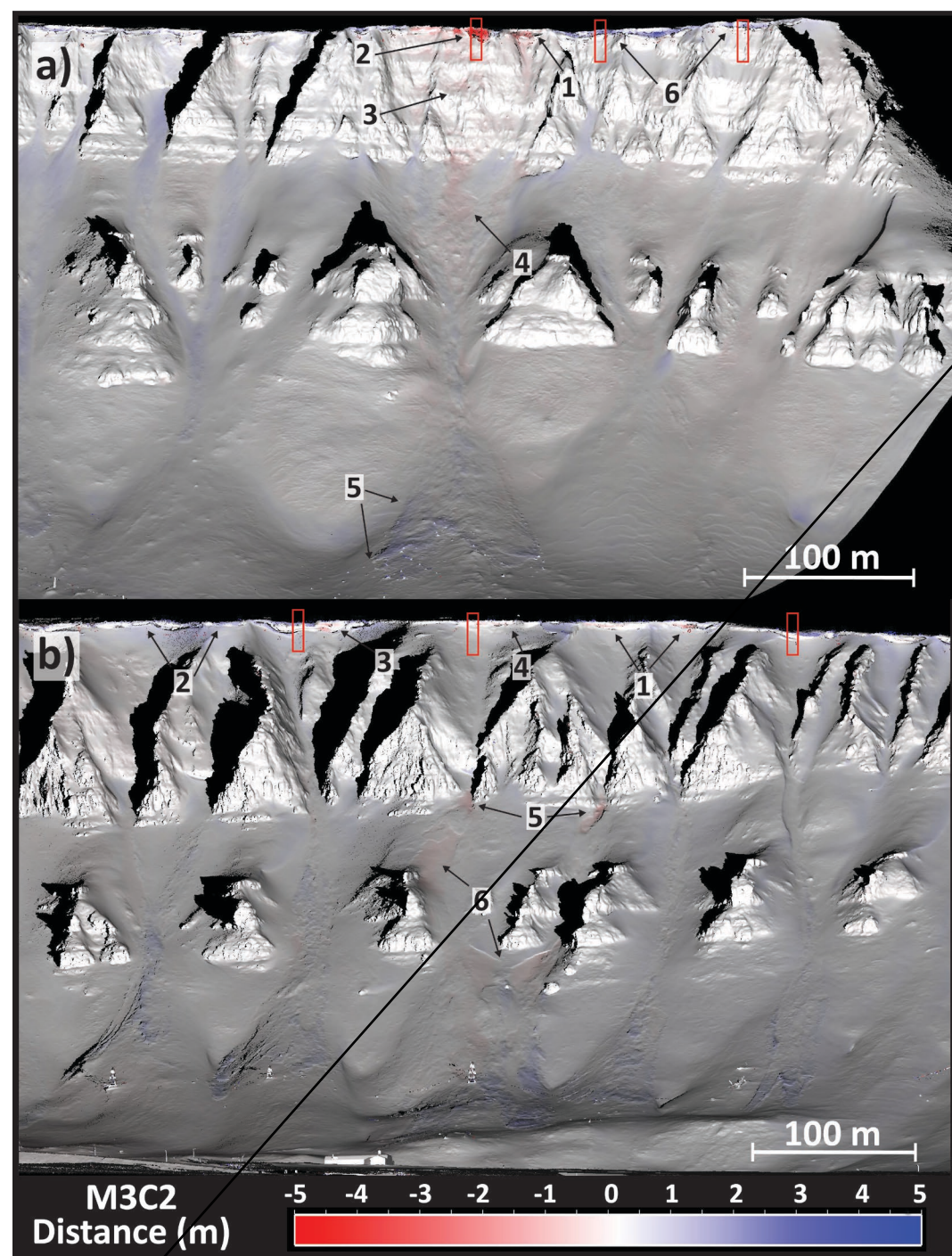
Figure 5. 2D cornice profiles showing cornice progression for selected scan dates throughout the 2016/2017 winter season. Each profile is labeled as referred to in the text and corresponds to the location and POV depicted in Figure 2

- Revise the color scheme of the profile to distinguish between the dates.

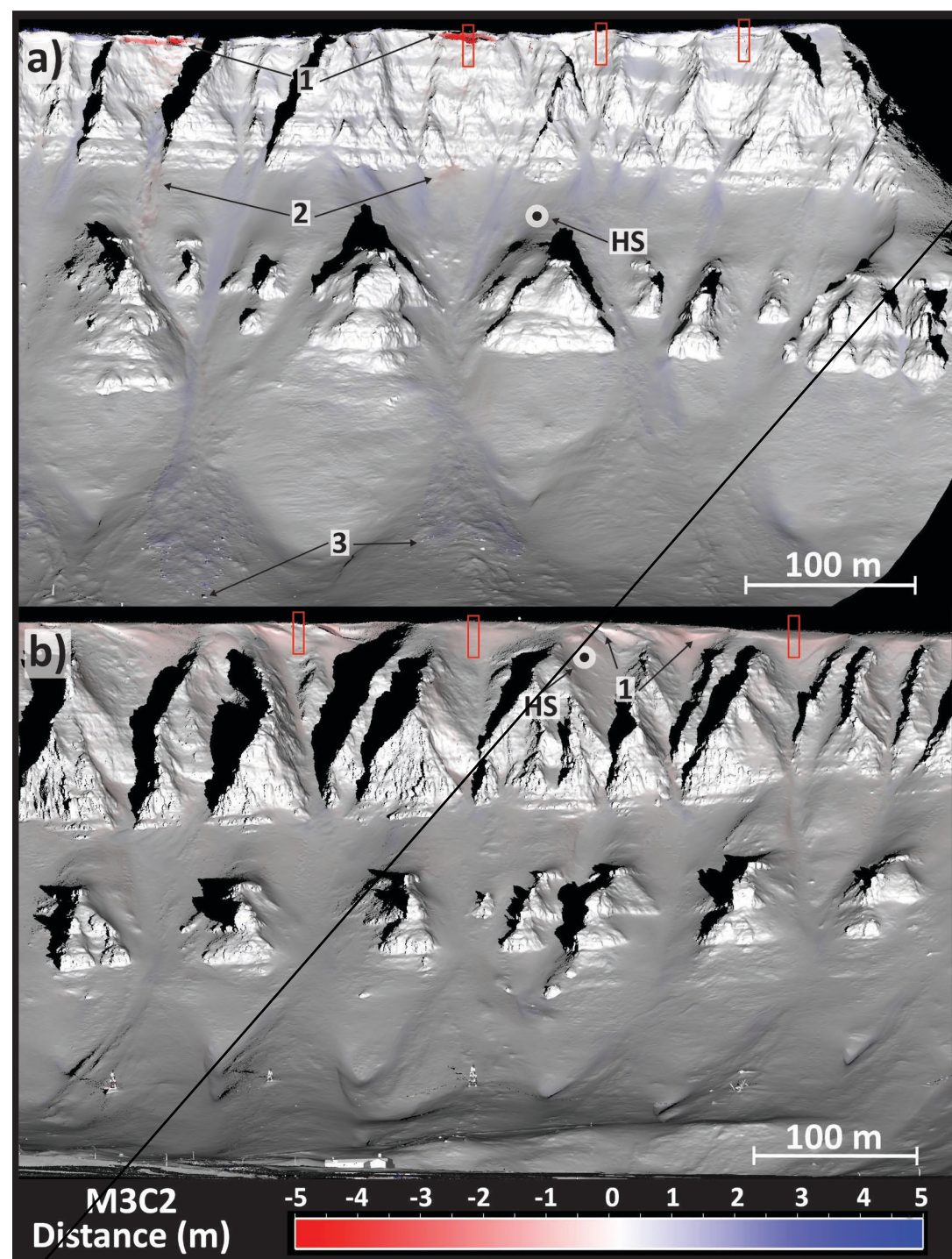


665

Figure 7 2D cornice profiles showing cornice progression for 2017/2018 winter season scan dates. Each profile is labeled as it referred to in the text and corresponds to the location and POV depicted in Figure 2.



675 **Figure 9.** M3C2 distances displaying changes to the snow cover on Gruvefjellet between the 21 March and 25 April 2018 scans (a) and on Platåberget between the 25 April and 1 May 2018 scans (b). Red rectangles in both panels indicate the locations of the cornice profiles. Specific snow surface features are annotated as they are referred to in the text.



685

Figure 12 M3C2 distances displaying changes to the snow cover on Gruvefjellet (a) and Platåberget (b) between the 2 March and 23 March scans. Red rectangles in both panels indicate the locations of the cornice profiles. Specific snow surface features are annotated as they are referred to in the text, and snow depth sensors are marked and labeled.